Steel and Composite Structures, Vol. 10, No. 1 (2010) 87-108 87
DOI: http://dx.doi.org/10.12989/scs.2010.10.1.087

A parametric study on buckling loads and tension field stress patterns of steel plate shear walls concerning buckling modes

P. Memarzadeh, M. Azhari* and M.M. Saadatpour

Department of Civil Engineering, Isfahan University of Technology, Isfahan, Iran, P.O. Box 84156-83111

(Received February 14, 2007, Accepted January 8, 2010)

Abstract. A Steel Plate Shear Wall (SPSW) is a lateral load resisting system consisting of an infill plate located within a frame. When buckling occurs in the infill plate of a SPSW, a diagonal tension field is formed through the plate. The study of the tension field behavior regarding the distribution and orientation patterns of principal stresses can be useful, for instance to modify the basic strip model to predict the behavior of SPSW more accurately. This paper investigates the influence of torsional and out-of-plane flexural rigidities of boundary members (i.e. beams and columns) on the buckling coefficient as well as on the distribution and orientation patterns of principal stresses associated with the buckling modes. The linear buckling equations in the sense of von-Karman have been solved in conjunction with various boundary conditions, by using the Ritz method. Also, in this research the effects of symmetric and anti-symmetric buckling modes and complete anchoring of the tension field due to lacking of in-plane bending of the beams as well as the aspect ratio of plate on the behavior of tension field and buckling coefficient have been studied.

Keywords: steel shear wall; shear buckling; anchoring; tension field; thin plate; Ritz method; principal stresses.

1. Introduction

A steel plate shear wall is a lateral load resisting system consisting of vertical steel plate infills connected to surrounding beams and columns in one or more bays along the full height of the structure. The infill plates can either be welded or bolted to the frame. In the past, design philosophy for the steel plate shear wall was based on the prevention of the plate buckling leading to the employment of thick infill plates or stiffener but later the designers preferred to employ unstiffened thin plates as to take advantage of the post-buckling capacity of the plate. The first major building employing the steel plate shear wall as a lateral load resisting system was Nippon Steel Building completed in 1970 in Tokyo (Astaneh-Asl 2001). Various specifications of the SPSWs such as lightness, high initial stiffness, ductility and economical advantages have acquired growing attentions.

Many researchers have been interested in studying the SPSWs. While performing experimental investigations on the thin aluminum shear panels of an aircraft, Wagner found out that in thin-webbed structures with stiff boundary members a diagonal tension field would be formed when buckling

* Corresponding Author, E-mail: mojtaba@cc.iut.ac.ir

occurs. Then Wagner (1931) developed the pure tension theory stating that the formation of the tension field is the primary mechanism for shear resistance. The incomplete tension field theory was later presented by Kuhn, *et al.* (1952). On the basis of Kuhn's theory the shear resistance capacity is a combination of pure shear and inclined tension field. These theories do not explain the extent, uniformity or non-uniformity and also the angle of inclination of the tension field and the affecting factors.

Modern design codes and standards are increasingly requiring an accurate assessment of inelastic structural response. While research institutions often use powerful and sophisticated software packages, they are not common in industry. Design engineers require the ability to assess inelastic structural response using conventional analysis software that is commonly available and is relatively simple to use (Shishkin, *et al.* 2005). An analytical model-termed the strip model-was developed by Thorburn, *et al.* (1983) to simulate the tension field behavior, wherein the infill plate is modeled as a series of tension-only strips at the same angle of inclination, θ, as the tension field (Fig. 1(a)). They derived the angle of inclination for the strips, θ, from the principle of Least Work as a function of axial stiffness of boundary members.

By including the effect of in-plane flexural stiffness of boundary members and employing the principle of Least Work, Timler and Kulak (1983) derived another equation for θ in terms of axial and flexural rigidities of surrounding members. From analytical and experimental tests, Timler and Kulak (1983) concluded that the calculated θ by their equation can better model the tension field behavior.

Many experimental tests were conducted by the researchers to examine the validity of the strip model. From these tests different results were reported. Tromposh and Kulak (1987) derived the conservative estimates of the initial stiffness and of ultimate capacity of the shear wall. Elgaaly, *et al.* (1993a,b and 1994) found the strip mode to be in good agreement with the test results for the ultimate capacity, but the initial stiffness was a little overestimated. By including the gravity forces, Driver, *et al*. (1997 and 1998a,b) found the strip model slightly underestimated the elastic stiffness of the test specimen, while providing excellent agreement with the ultimate strength. Lubell (1997) Lubell, *et al*. (2000) found the strip model to be inconsistent with the test results. He found that the strip model can not describe the envelope pushover behavior of any of his four-storey specimens accurately. Using plastic analysis theory and the assumption of discrete strips to represent the infill plate, Berman and Bruneau (2003) derived equations to calculate the ultimate strength of SPSW. This equation was found to underestimate the experimental capacities. To reflect the non-uniformity of the tension field, Rezai Rezai (1999) and Rezai, *et al.* (2000) developed another strip model (Fig. 1(b)). This model had a higher estimated elastic stiffness and ultimate capacity compared to the conventional strip model.

The Canadian Steel Design Standard (2001) suggests the application of the strip model as a design tool for steel plate shear wall (CAN/CSA 516-01) and Eq. (2) for the calculation of θ (clause 20.3.1). However, researchers are still searching for an increase in the precision of the prediction of the overall behavior of the shear wall.

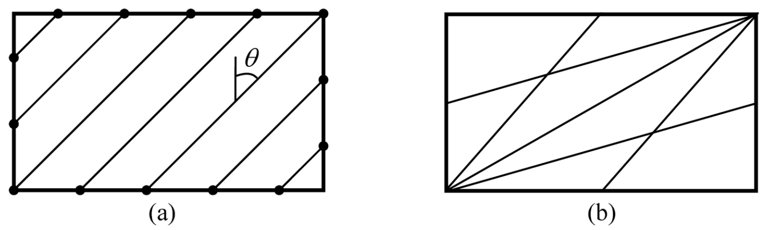

Fig. 1 Analytical strip models developed by (a) Thorburn, *et al*. (1983) and (b) Rezai (1999)

This paper investigates the effect of different parameters on buckling load as well as on the distribution and orientation patterns of the tension field principal stresses. These parameters include torsional and out-of-plane flexural rigidities of boundary members, anchoring of the tension field, plate aspect ratio and the symmetry of buckling modes.

In the present work, the Ritz method (Reddy 2002) is used to establish an eigenvalue problem for the buckling analysis of an isotropic plate with different boundary conditions. The von-Karman theory (Varadan and Bhaskar 1999) is employed for the modeling of the plate flexure. The torsional and out-of-plane flexural rigidities of the boundary members are modeled by the springs which were continuously and properly positioned along the edges of the plate.

2. Theory

2.1 Modeling of SPSW

The three-dimensional analysis of the SPSW is time-consuming and complex. In thin steel plates the thickness is very small compared to other dimensions. Thus, one may simplify the three-dimensional problem to a two-dimensional model to simplify the analyses.

The surrounding members are modeled by the springs. To define logical parameters for the amounts of torsional and out-of-plane flexural rigidities of surrounding members, the non-dimensional stiffness parameters α and β are introduced as follows:

$$\alpha = \frac{K_{tor}}{D}$$

$$B = \frac{K_{flx}}{D} \tag{1}$$

where K_{tor}, K_{flx} are the unit length torsional and out-of-plane flexural rigidities of surrounding members, respectively. Two models are defined for studying the effects of two stiffness parameters α and β, separately (Fig. 2). In Models 1 and 2, the torsional and out-of-plane flexural rigidities of surrounding members are accounted, respectively. This way, a comparison between the effectiveness of different stiffness parameters of surrounding members is carried out.

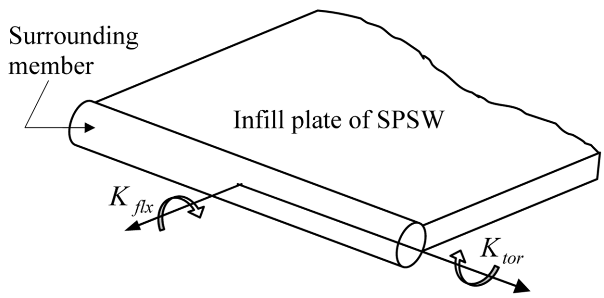

Fig. 2 General scheme for a section of Models 1 and 2

Modeling of a single SPSW and a SPSW belonging to an intermediate floor of a multi-storey frame may need to be considered differently. This is because the beams of the later SPSW are shared out by the other SPSWs and then may not bend while the beams of a single SPSW are free to bend, relatively. The lacking of the in-plane beams bending causes the complete anchoring of the tension field. Thus, for this type of tension field anchoring, we will treat the following two cases: I– the beams are free to bend; II– the beams may not bend.

2.2 Ritz method

This paper utilizes the Ritz method to analyze the buckling of infill plate of a SPSW under an applied in-plane shear loading (Fig. 3).

The elastic (U) and the geometric strain energy (V_p) are the variants used in the energy solution, and are given by the following equations:

$$U = U_p + U_s \tag{2}$$

where U_p and U_s are the plate and spring elastic strain energy, respectively, defined as below:

$$U_p = \frac{D}{2}\int_A [(w_{,xx} + w_{,yy})^2 - 2(1-\nu)(w_{,xx}w_{,yy} - w_{,xy}^2)]dA \tag{3}$$

$$\begin{aligned} U_s = & \int\left[\frac{K_{tor}}{2}\left(w_{,x}^2\Big|_{x=-\frac{a}{2}} + w_{,x}^2\Big|_{x=\frac{a}{2}}\right) + \frac{K_{flx}}{2}\left(w_{,y}^2\Big|_{x=-\frac{a}{2}} + w_{,y}^2\Big|_{x=\frac{a}{2}}\right)\right]dy \\ & + \int\left[\frac{K_{tor}}{2}\left(w_{,y}^2\Big|_{y=-\frac{b}{2}} + w_{,y}^2\Big|_{x=\frac{b}{2}}\right) + \frac{K_{flx}}{2}\left(w_{,x}^2\Big|_{y=-\frac{b}{2}} + w_{,x}^2\Big|_{y=\frac{b}{2}}\right)\right]dx \end{aligned} \tag{4}$$

in which D, A and w are the flexural rigidity, the area and the lateral buckling displacement of the plate, respectively. The comma denotes differentiation with respect to the corresponding co-ordinates.

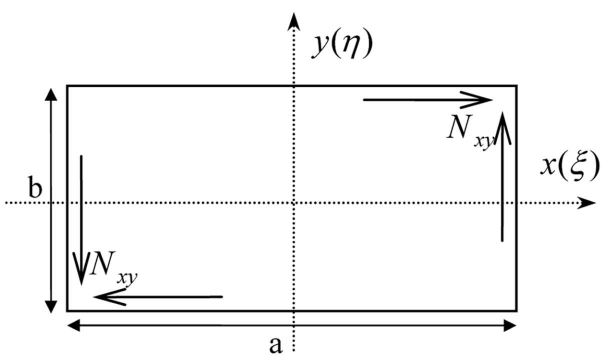

Fig. 3 Isotropic plate under pure shear

$$V_p = -N_{xy}\int_A (w_{,x}w_{,y})dA \tag{5}$$

where N_{xy} is the elastic shear buckling load. In the use of the Ritz method, an appropriate displacement function for w must be chosen. That used herein is the polynomial-based displacement function which consists of a boundary polynomial specifying the geometric and kinematic boundary conditions multiplied by a complete simple polynomial. This displacement function is written in general form for both the Models 1 and 2 as follows:

$$w = \varphi_{b1}(\xi, \eta)\sum_{q=0}^{p}\sum_{r=0}^{q} a_{1m}\phi_{1m}(\xi, \eta) + \varphi_{b2}(\xi)\sum_{n=1}^{f_2} a_{2n}\phi_{2n}(\xi) + \varphi_{b3}(\eta)\sum_{l=1}^{f_3} a_{3l}\phi_{3l}(\eta) \tag{6}$$

where p is the degree of a two-dimensional polynomial and a_{1m}, a_{2n}, a_{3l} are the arbitrary Ritz coefficients. $\phi_{1m}(\xi,\eta)$ is the m-th term of a two-dimensional polynomial as below (Smith, *et al.* 1999):

$$\phi_{1m}(\xi, \eta) = \xi^r\eta^{q-r} \tag{7}$$

in which $\xi = 2x/a$, $\eta = 2y/b$. The value of the m-th term is given by:

$$m = \frac{(q+1)(q+2)}{2} - r \tag{8}$$

$\phi_{2n}(\xi)$, $\phi_{3l}(\eta)$ are one-dimensional polynomials expressed by:

$$\phi_{2n}(\xi) = \xi^n$$
$$\phi_{3l}(\eta) = \eta^l \tag{9}$$

The number of degrees of freedom in the two-dimensional polynomial $\phi_{1m}(\xi,\eta)$ is given by:

$$f_1 = \frac{(p+1)(p+2)}{2} \tag{10}$$

and also, f_2 and f_3 are the numbers of degrees of freedom for the one-dimensional polynomials $\phi_{2n}(\xi)$ and $\phi_{3l}(\eta)$ which can be arbitrarily chosen, respectively.

The terms $\varphi_{b1}(\xi,\eta)$, $\varphi_{b2}(\xi)$ and $\varphi_{b3}(\eta)$ are the boundary polynomials describing the boundary conditions defined in Table 1.

In the buckling analysis, the kinematic and geometric boundary conditions are specified when the boundary polynomials $\varphi_{b1}(\xi,\eta)$, $\varphi_{b2}(\xi)$ and $\varphi_{b3}(\eta)$ are multiplied by the corresponding internal interpolation polynomials.

Table 1 Boundary polynomials for various models and cases

		$\varphi_{b1}(\zeta,\eta)$	$\varphi_{b2}(\zeta)$	$\varphi_{b3}(\eta)$
Model1	Case I	$(\xi-1)^1(\xi+1)^1(\eta-1)^1(\eta+1)^1$	0	0
	Case II	$(\xi-1)^1(\xi+1)^1(\eta-1)^2(\eta+1)^2$	0	0
Model2	Case I	$(\xi-1)^1(\xi+1)^1(\eta-1)^1(\eta+1)^1$	$(\xi-1)^1(\xi+1)^1$	$(\eta-1)^2(\eta+1)^2$
	Case II	$(\xi-1)^1(\xi+1)^1(\eta-1)^2(\eta+1)^2$	$(\xi-1)^1(\xi+1)^1$	$(\eta-1)^2(\eta+1)^2$

2.3 Linear eigenvalue analysis

Eq. (6) can be re-written in the matrix form as follow:

$$w = \mathbf{a}^{\mathrm{T}}\mathbf{\Phi} \tag{11}$$

in which $\mathbf{a}$, $\mathbf{\Phi}$ are defined as below:

$$\mathbf{a} = \{[a_{1m}]_{1\times f_1}, [a_{2n}]_{1\times f_2}, [a_{3l}]_{1\times f_3}\}^T \tag{12}$$

$$\mathbf{\Phi} = \{[\varphi_{b1}(\xi,\eta)\phi_{1m}(\xi,\eta)]_{1\times f_1}, [\varphi_{b2}(\xi)\phi_{2n}(\xi)]_{1\times f_2}, [\varphi_{b3}(\eta)\phi_{3l}(\eta)]_{1\times f_3}\}^T \tag{13}$$

where ($m = 1, 2, ..., f_1$), ($n = 1, 2, ..., f_2$) and ($l = 1, 2, ..., f_3$).

The total potential energy Π of the system is given by:

$$\Pi = U + V_p \tag{14}$$

Based on the principle of minimum potential energy, the total potential Π in Eq. (14) is minimized with respect to the unknown Ritz coefficients a_{1m}, a_{2n} and a_{3l}. Because Π is a function of the product of Ritz coefficients, minimization by formal differentiation leads to a set of simultaneous linear independent equations which may be written in the matrix form as follows:

$$(\mathbf{K}_0 - N_{xy}\mathbf{K}_{\mathrm{G}})\mathbf{a} = 0 \tag{15}$$

where $\mathbf{K}_0$ and $\mathbf{K}_{\mathbf{G}}$ are the linear and geometric stiffness matrices, respectively. These stiffness matrices are given in Appendix.

The solution of these equations produced the eigenvalues (buckling loads) and substituting of the corresponding eigenvectors into the displacement function w in Eq. (6) as the Ritz coefficients gives the buckling modes.

2.4 Stress analysis

Since the buckling modes of a plate specify the proportional values of transverse deflections, the corresponding values of strains and stresses will be calculated proportionally. Using the transverse deflection w, the stresses in the mid-plane of plate can be written by:

$$\begin{aligned} \sigma_x &= \frac{E}{2(1-\nu^2)}(w_{,x}^2 + \nu w_{,y}^2) \\ \sigma_y &= \frac{E}{2(1-\nu^2)}(w_{,y}^2 + \nu w_{,x}^2) \\ \tau_{xy} &= G w_{,x} w_{,y} \end{aligned} \tag{16}$$

where G is the shear modulus of elasticity. Using the Mohr's circle (Budynas 1977), the state of stresses can be represented in the principal coordinates. Also the angle of inclination of the tension field can be calculated by determining the orientation of the principal stresses. Then, it is possible to plot the distribution and orientation patterns of the principal stresses in the tension field of a plate.

3. Numerical parametric studies

3.1 General

The objective of this parametric study is to investigate the effect of different factors on shear buckling coefficient and tension field behavior of the infill plate of SPSW. The parameters under study include: torsional and out-of-plane flexural rigidities of boundary members, symmetric and anti-symmetric buckling modes, increasing the anchoring of the tension field due to lacking of in-plane bending of the beams and aspect ratio of plate. The torsional and out-of-plane flexural rigidities of the boundary members are modeled by appropriate springs in Models 1 and 2, respectively. The complete anchoring of the tension field is accounted in Case II, while is ignored in Case I. A computer program has been developed based on the von-Karman theory and the Ritz method. The program is flexible to analyze the buckling of the various models and cases. To verify the results of the buckling analysis comparisons are made with the available references.

3.2 Buckling analysis

The numerical analyses were performed on Models 1 and 2 by the computer program for Cases I and II. In these buckling analyses, the values of f_2, f_3 and p were selected equal to 8. To compare the various buckling analyses, the non-dimensional buckling coefficient was employed as follows:

$$k_s = \frac{N_{xy} b^2}{\pi^2 D} \tag{17}$$

The solution of eigenproblem equations results in eigenvalues and corresponding eigenvectors. By plotting the various buckling mode shapes, it will be specified which modes are symmetric or anti-symmetric.

The "first" symmetric and anti-symmetric modes correspond to the minimum values of the symmetric and anti-symmetric buckling loads, respectively. However, in this paper the word "first" is omitted for brevity.

3.2.1 Verification of buckling analysis

With the purpose of verifying the validity of buckling analyses, the results are compared with the available references. The stiffness of springs is selected equal to zero or infinite for modeling simply support (S) or clamped edges (C), respectively. When $\alpha = 0$ or $\beta = \infty$, the boundary conditions of the plate are SSSS for Case I and CCSS for Case II. Also, when $\alpha = \infty$, the plate boundary condition is CCCC for both cases I and II. In the following Tables 2 and 3, the resulting buckling coefficients from the present analyses are compared with those reported in references. As the Tables 3 and 4 show, the results are in good agreement.

Table 2 Comparison the present results for Model 1 with those of available reference

	$\alpha = \frac{K_{tor}}{D}$	Boundary Conditions	a/b	k_s Present Symmetric	Present Anti-symmetric	Timoshenko and Gere (1963)
Case I	$\alpha = 0$	SSSS	1.0	9.3254	11.5484	9.34
			1.5	7.0707	7.9591	7.10
			2.0	6.5464	6.5781	6.60
			3.0	5.9535	5.8465	5.90
	$\alpha = \infty$	CCSS	1.0	14.6515	17.1165	14.71
			1.5	11.4791	12.0293	11.50
			2.0	10.6527	10.5545	10.34
			3.0	9.8449	10.6985	-------
Case II	$\alpha = 0$	CCSS	1.0	12.5662	14.2067	12.28
			1.5	11.1291	10.7849	11.12
			2.0	10.1971	10.0107	10.21
			3.0	9.4928	9.5609	9.61
	$\alpha = \infty$	CCCC	1.0	14.6403	16.9289	14.71
			1.5	11.4596	11.8110	11.50
			2.0	10.5854	10.2617	10.34
			3.0	9.5574	9.7442	-------

Table 3 Comparison the present results for Model 2 with those of available reference

	$\beta = \frac{K_{flx}}{D}$	Boundary Condition	a/b	k_s Present Symmetric	Present Anti-symmetric	Timoshenko and Gere (1963)
Case I	$\beta = \infty$	SSSS	1.0	9.3245	11.5424	9.34
			1.5	7.0701	7.9563	7.10
			2.0	6.5458	6.5767	6.60
			3.0	5.9531	5.8460	5.90
Case II	$\beta = \infty$	CCSS	1.0	12.5658	14.2002	12.28
			1.5	11.1290	10.7828	11.12
			2.0	10.1971	10.0103	10.21
			3.0	9.4928	9.5605	9.61

3.2.2 Results of buckling analysis

Typically, the symmetric and anti-symmetric buckling modes of plates with the aspect ratios of 1 and 3 (Model 1) are depicted in three-dimensional views (Fig. 4).

Figs. 5-8 show the effect of varying the stiffness parameters α and β on the symmetric and anti-symmetric buckling coefficients of plates for both Cases I and II.

The following observations could be made from these figures:

- The symmetric buckling load of a plate with an aspect ratio equal or greater than 1.5 is close to that for its anti-symmetric mode.
- Although the symmetric buckling mode is often the critical mode of shear buckling, sometimes the anti-symmetric mode would be critical.
- Figs. 5 and 6 show that the shear buckling mode of plate would not be changed by varying the

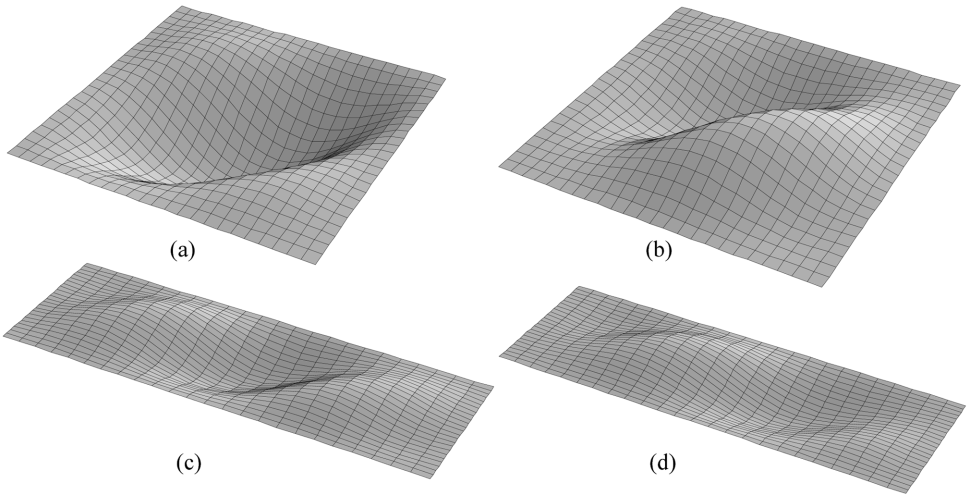

Fig. 4 Symmetric (a,c) and anti-symmetric (b,d) shear buckling modes for Model 1 and aspect ratios 1, 3

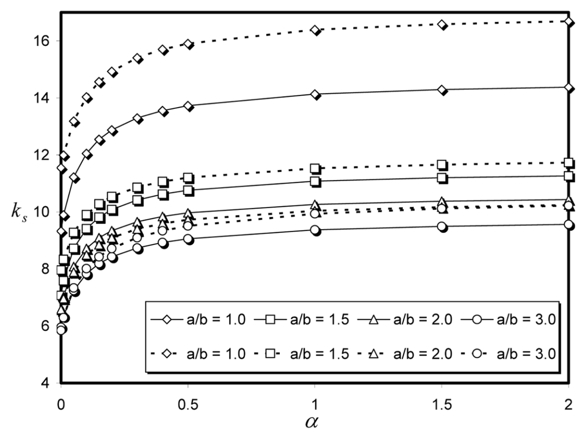

Fig. 5 Shear buckling coefficient v.s. α for Model 1, Case I (line for symmetric and dashed for anti-symmetric buckling)

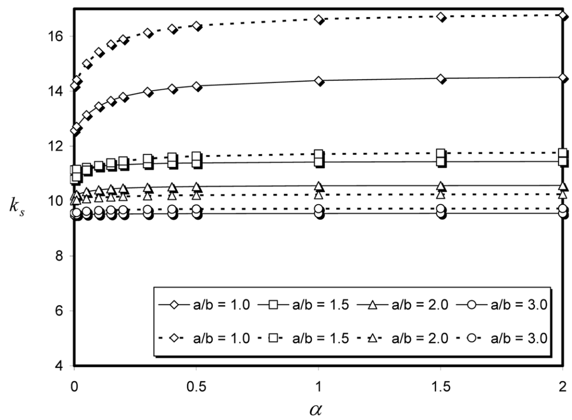

Fig. 6 Shear buckling coefficient v.s. α for Model 1, Case II (line for symmetric and dashed for anti-symmetric buckling)

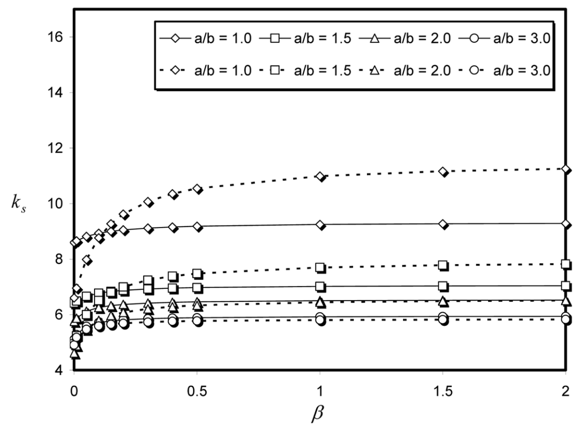

Fig. 7 Shear buckling coefficient v.s. β for Model 2, Case I (line for symmetric and dashed for anti-symmetric buckling)

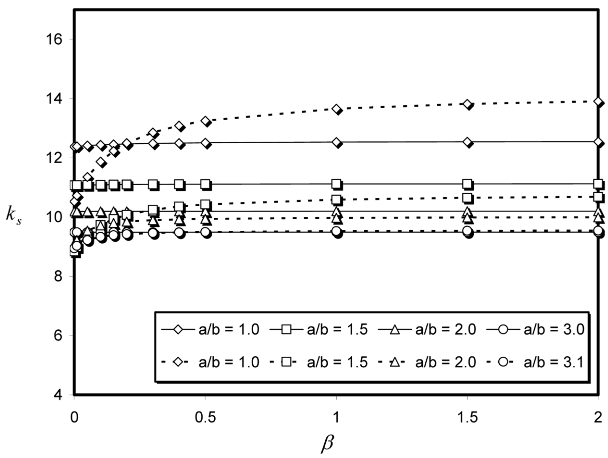

Fig. 8 Shear buckling coefficient v.s. β for Model 2, Case II (line for symmetric and dashed for anti-symmetric buckling)

stiffness parameter α; because there is no intersection for curves in Figs. 5 and 6.

- Figs 7 and 8 show that the variation of amounts of the stiffness parameter β may change the shear buckling mode of plate.
- The buckling coefficients of Case II are greater than those for Case I.

3.3 Results of stress analysis

3.3.1 Principal stress distribution pattern (PSDP)

By comparing the PSDPs with the corresponding buckling modes, the areas where the amounts of principal stresses are peak, may be specified. Figs. 9 and 10 illustrate these comparisons for two

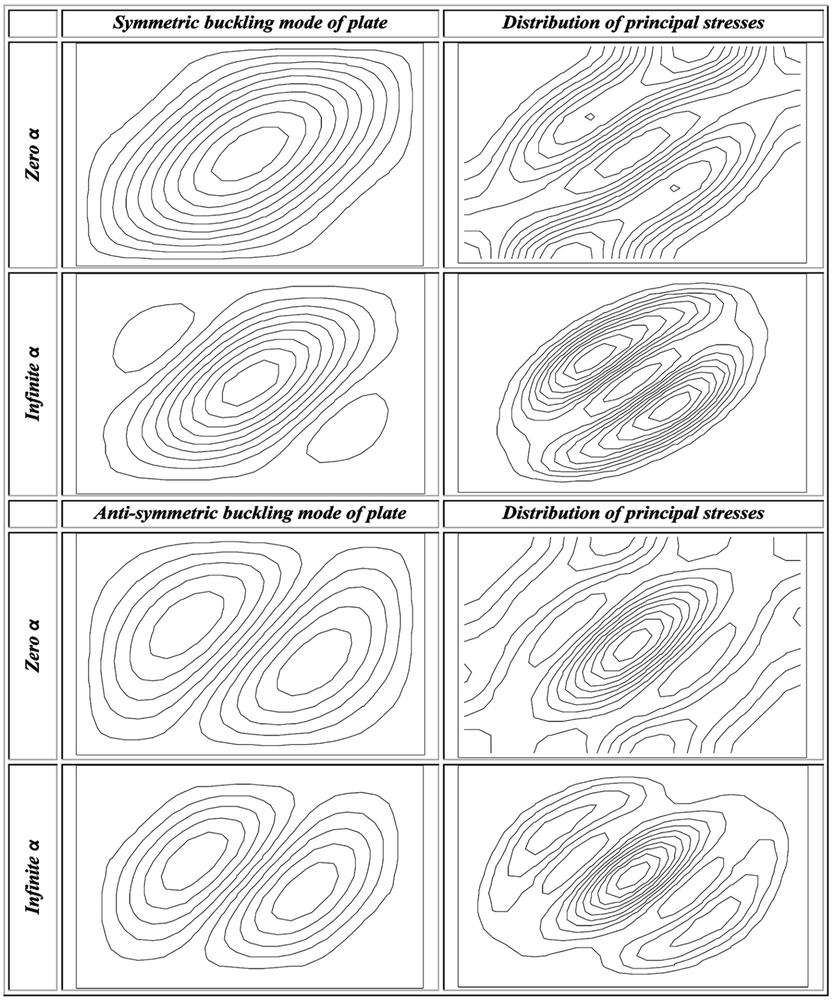

Fig. 9 Symmetric and anti-symmetric buckling mode shapes and PSDPs for two extremes of and $\alpha = 0$ $\alpha = \infty$ (Model 1, Case I and aspect ratio 1.5)

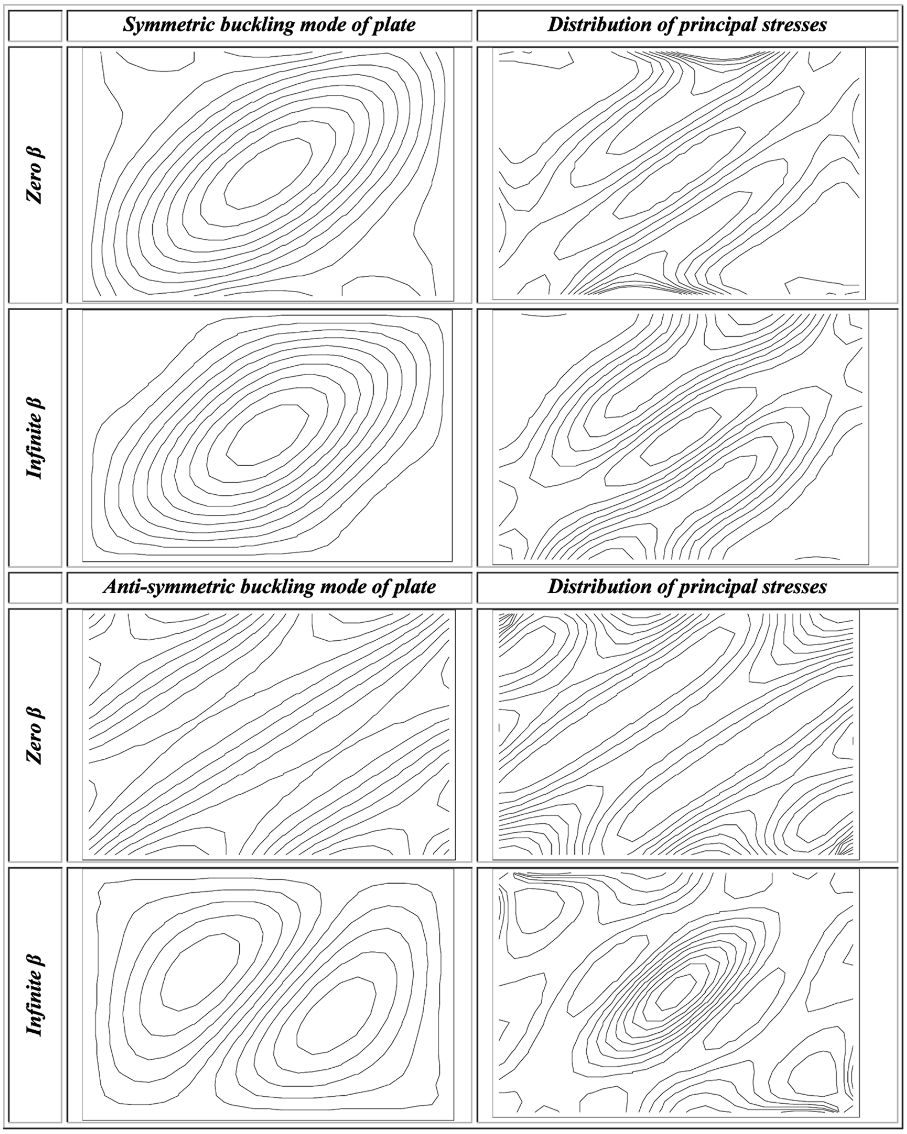

Fig. 10 Symmetric and anti-symmetric buckling mode shapes and PSDPs for two extremes of $\beta = 0$ and $\beta = \infty$ (Model 2, Case I and aspect ratio 1.5)

extreme values of zero and infinite for the stiffness parameters α and β. These figures show that the peak(s) of principal stresses occurs at the slope(s) of buckling mode shapes for both symmetric and anti-symmetric modes. Therefore, in symmetric buckling modes, the principal stresses peaks are at both sides of the plate center, while in anti-symmetric buckling this peak would be in the center of the plate. Also, Figs. 9 and 10 show that the PSDPs are symmetric for both symmetric and anti-symmetric buckling modes.

For showing some patterns simultaneously, it is advantageous that the patterns are put together and combined as shown in Fig. 11. The buckling mode shapes as well as the PSDPs related to various

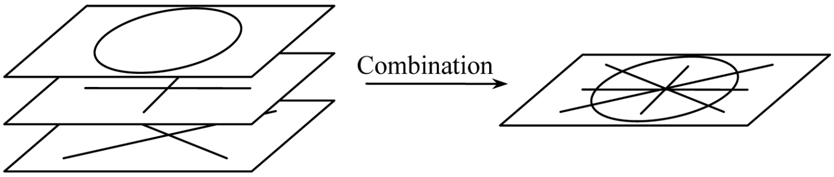

Fig. 11 Scheme for combination of some patterns

values of the stiffness parameters α and β, were combined in Fig. 12. This figure shows that the locations of the deflection and principal stress peaks would not be noticeably changed by varying the stiffness parameters α and β.

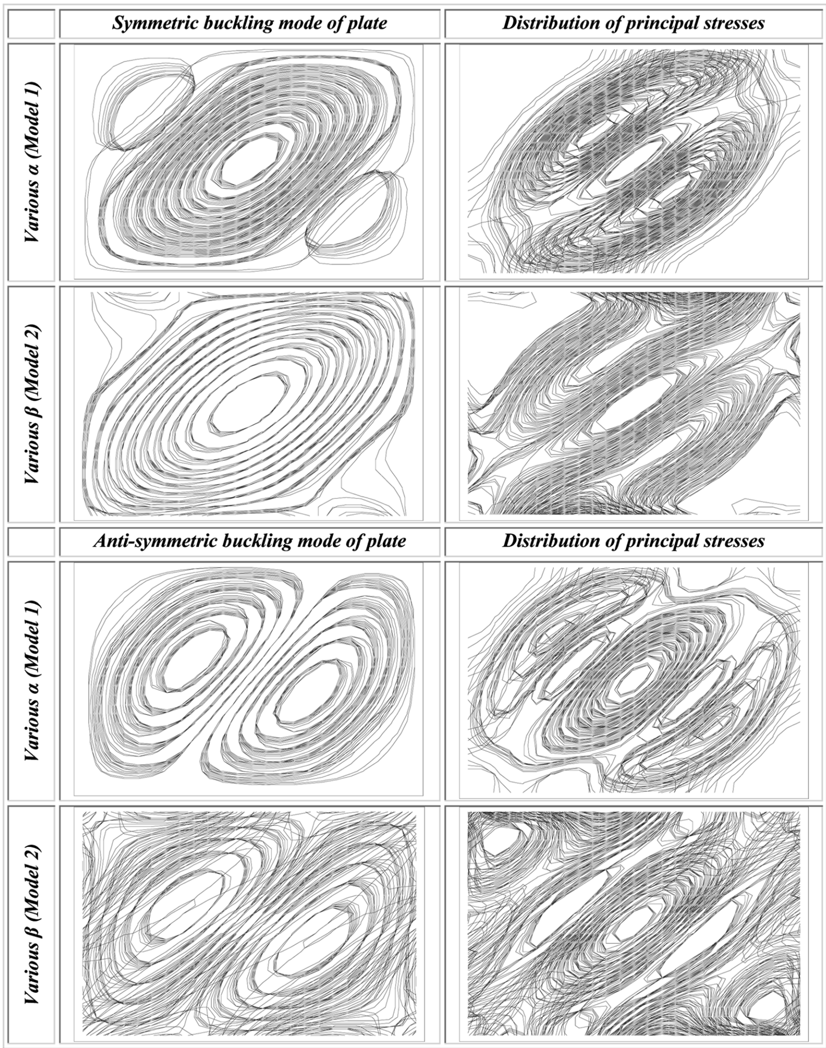

Fig. 12 Combination of buckling mode shapes and combination of PSDPs related to various α and β for Models 1 and 2, respectively (Case I and aspect ratio 1.5)

3.3.2 Principal stress orientation pattern (PSOP)

The orientations of principal stresses can be determined at each point of the plate by using the Mohr's circle. Figs. 13 and 14 show the combined PSOPs related to various values of stiffness parameters α and β, respectively. In these figures, the orientation of each depicted line represents the orientation of the related principal stress. By careful observation, it is realized that:

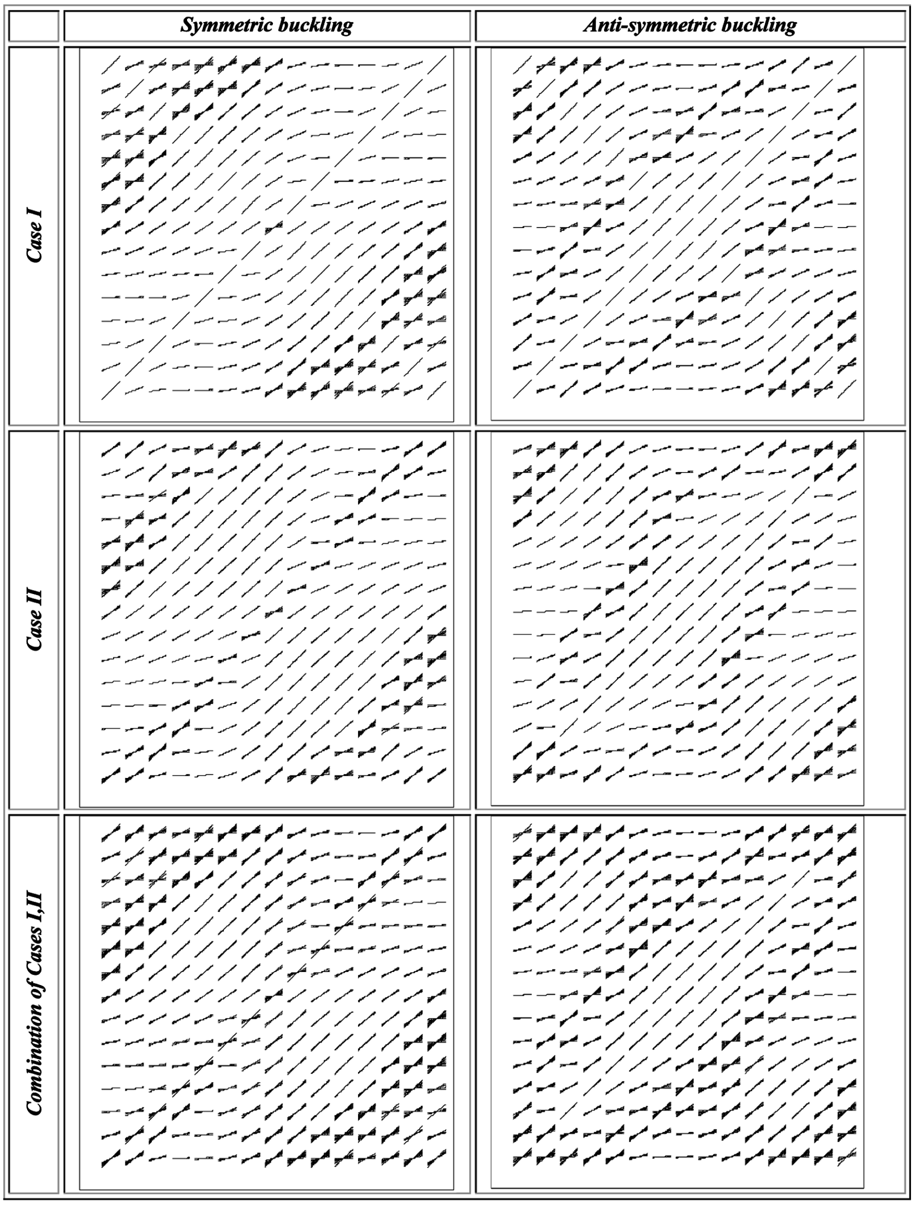

Fig. 13 Combination of PSOPs related to various α (Model 1 and aspect ratio 1)

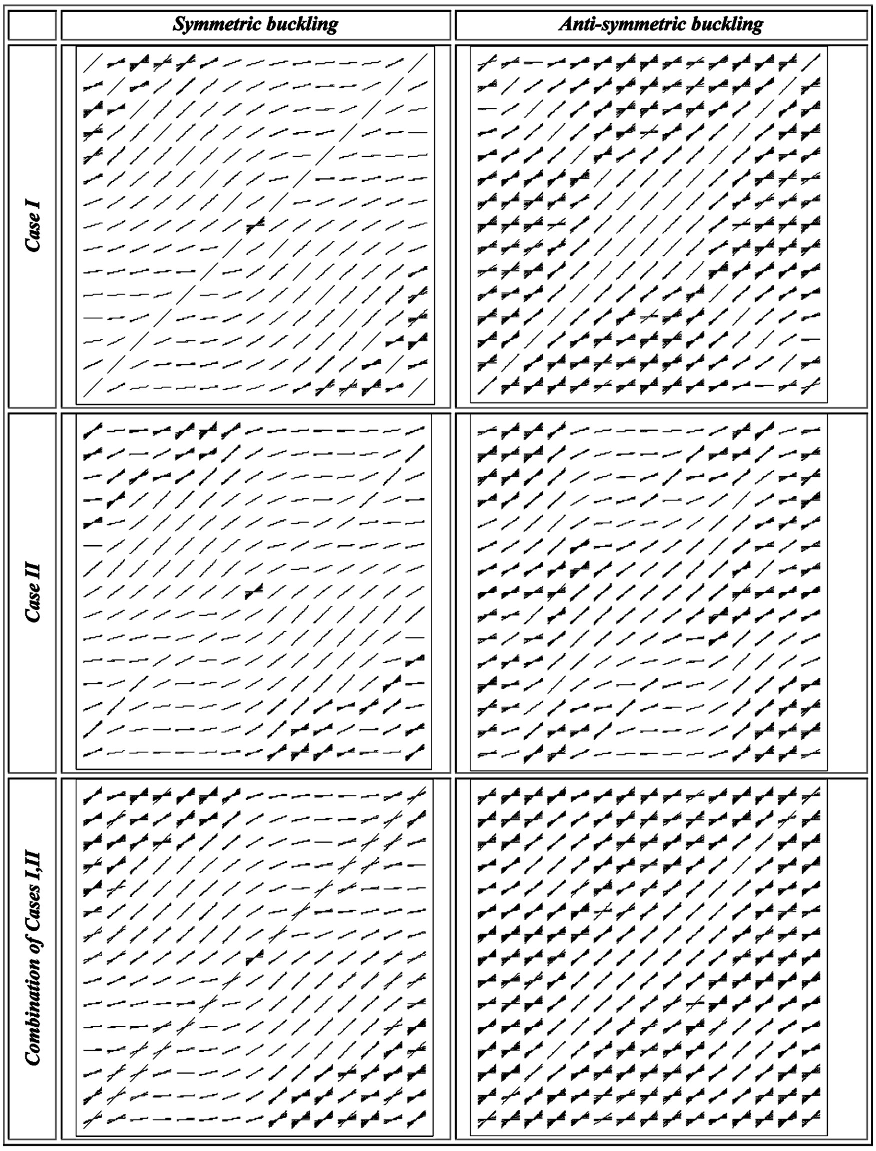

Fig. 14 Combination of PSOPs related to various β (Model 2 and aspect ratio 1)

- Associated with the buckling modes, there are areas in the plate where the orientations of related principal stresses will not be changed by varying the values of the stiffness parameters α or β. These areas of the plate in symmetric buckling are more extended than those in anti-symmetric buckling. Also, these areas have different distribution for the symmetric and anti-symmetric buckling modes.
- The complete anchoring of the tension field due to lacking of in-plane bending of the beams has a slight effect on the orientations of the principal stresses. This conclusion is derived by observation of the combined patterns related to Cases I and II.

Fig. 15 shows the combinations of PSOPs related to symmetric and anti-symmetric buckling modes. This figure reveals that the PSOPs are relatively different for the symmetric and anti-symmetric buckling modes.

Typically, Fig. 16 shows the combination of the PSDP and PSOP of a plate. As it is observed, the orientations of principal stresses remain unchanged in the areas where the great stresses exist. There is the same result for other model or case, but these are not shown here for brevity.

The PSOPs of the plates with different aspect ratios are shown in Figs. 17 and 18. These figures reveal that the same results discussed above are nearly applicable for the plates with the various aspect ratios.

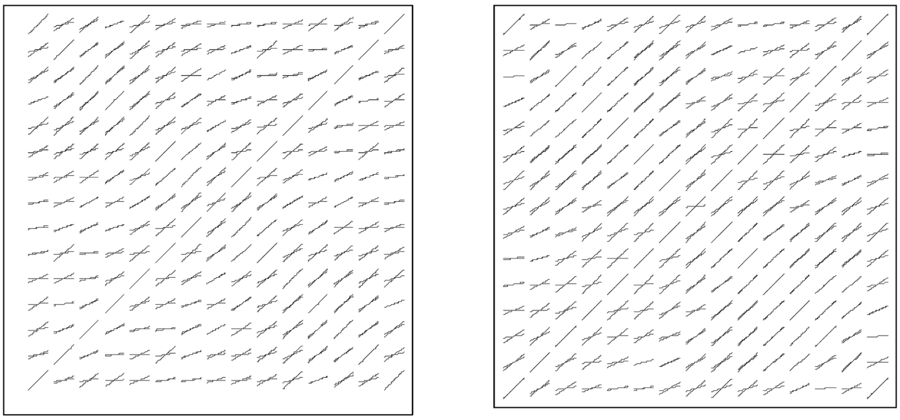

(a) (b)

Fig. 15 Combination of PSOPs related to symmetric and anti-symmetric buckling modes for (a) Model 1 and (b) Model 2 (Case I, $\alpha = 0$ and $\beta = 0$)

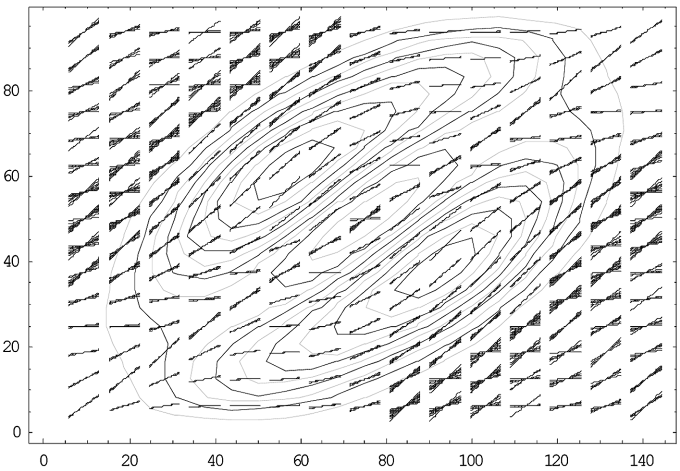

Fig. 16 Combination of PSDPs and PSOPs related to various α (Model 1, Case I, symmetric buckling and aspect ratio 1.5)

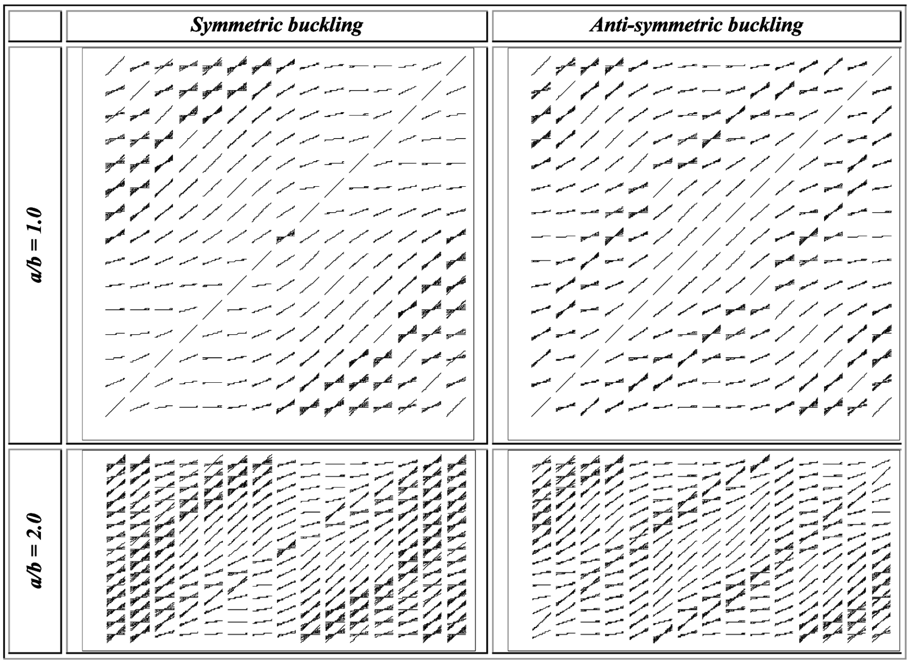

Fig. 17 Combination of PSOPs related to various α (Model 1, symmetric buckling and aspect ratios 1 and 2)

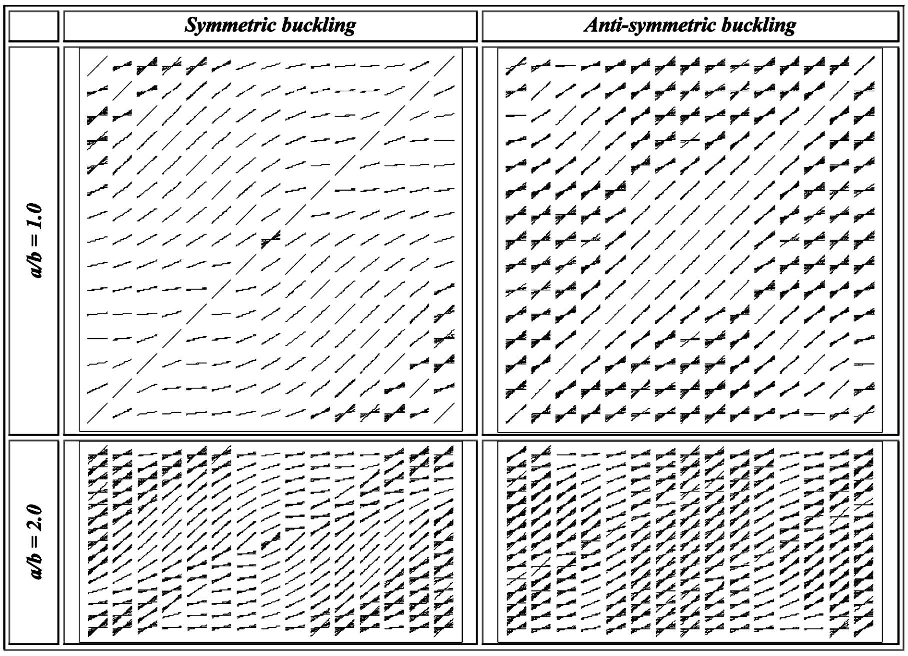

Fig. 18 Combination of PSOPs related to various β (Model 2, symmetric buckling and aspect ratios 1 and 2)

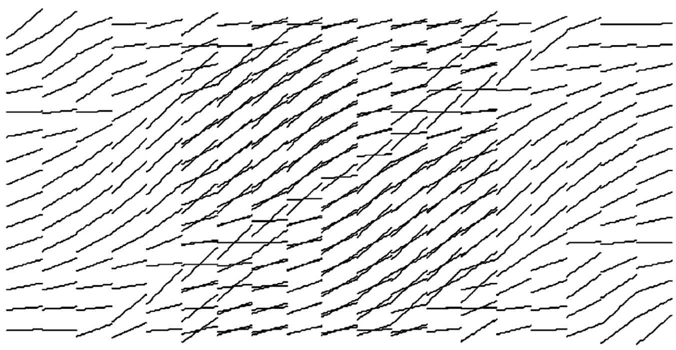

Fig. 19 Combination of PSOPs related to plates with aspect ratios 1 and 2 (Model 1 and symmetric buckling)

In Fig. 19, the PSOPs related to the two plates with different aspect ratios 1 and 2 are combined in order to better observe the difference between the PSOPs for these plates. It is clearly realized that the aspect ratio of the plate has slight effect on the PSOPs.

4. Conclusions

The present paper investigates the effect of different parameters on buckling coefficient and behavior of the tension field stresses in SPSW. These parameters include out-of-plane flexural and torsional rigidities of boundary members, symmetric and anti-symmetric buckling modes, tension field anchoring due to lacking of in-plane beams bending and aspect ratio of the plate.

The observations reveal that the variation of the out-of-plane flexural stiffness of boundary members, unlike for the torsional stiffness of boundary members, may change the critical shear buckling mode of plate; moreover, although the critical shear buckling mode of plate is often symmetric, sometimes the anti-symmetric mode would be critical.

Based on this research, the symmetric buckling load of a plate with an aspect ratio equal or greater than 1.5 is close to that for its anti-symmetric mode. For such a plate, the postbuckling mode may be a function of its initial imperfection; because initial imperfection of plates due to their fabrication causes that the plates do not experience the buckling bifurcation point and hence initial imperfections may play a role in determining which postbuckling modes of symmetric or anti-symmetric would occur. This role would be significant for plates with close symmetric and anti-symmetric buckling loads. As a result, it seems that the initial imperfection of plate should be considered as a parameter in developing the strip model, especially for a plate with aspect ratio equal or greater than 1.5. This parameter has not been included in any analytical models presented so far.

This research discusses the distribution and orientation patterns of principal stresses due to only out-of-plane displacements of plate associated with buckling modes. It is shown that the peak(s) of the principal stresses occurs at the slope(s) of buckling mode shapes for both symmetric and anti-symmetric modes; thus in symmetric buckling modes, the principal stresses peaks are at both sides of the plate center, while in anti-symmetric buckling this peak would be in the center of the plate. The locations of the deflection and principal stress peaks would not be noticeably changed by varying the torsional and out-of-plane flexural rigidities of boundary members. In addition, the principal stress distribution patterns (PSDPs) are symmetric for both symmetric and anti-symmetric buckling modes.

This paper shows that the principal stress orientation patterns (PSOPs) corresponding to the symmetric and anti-symmetric buckling modes of a plate are different, relatively. Since the angle of inclination of the tension field of a SPSW is an effective parameter on development of the strip model, the difference between these orientation patterns may be vital in modifying the strip model.

This study also revealed that variation of amounts of torsional or out-of-plane flexural rigidities of boundary members do not change the orientations of principal stresses in areas of the plate where located in the slopes of the buckling mode shapes and have relatively great principal stresses. Therefore, the torsional and out-of-plane digidities of boundary elements probably are not of primary parameters in development of the strip model.

The research carried out in this paper shows that the increase of the tension field anchoring of SPSWs in multi-storey frames due to lacking of the in-plane beam bending causes an increase in the shear buckling loads and has a slight effect on the PSOPs. The aspect ratio of plate has slight effect on the PSOPs. The same results discussed above are nearly applicable for the plates with the various aspect ratios. It should be noted that all results presented here for PSDPs and PSOPs are associated with buckling modes and based on the stresses due to only out-of-plane displacements of plate and further research is recommended to evaluate the validity of the results for the cases in which the total stresses are considered.

5. Recommendations for further research

This research focuses on qualitative study of the infill plate stresses of SPSWs associated with buckling modes. These stresses are due to only out-of-plane displacements of infill plates. Further research is recommended to incorporate either the pre-buckling stresses or the post-buckling stresses arising from the linear post-buckling membrane strains. Also, the effect of plasticity of the infill plate material on stress patterns could be studied. Further investigation is recommended to determine and include the role of the initial imperfection of infill plates as a parameter in developing the analytical strip models.

References

Astaneh-Asl, A. (2001), *Seismic behavior and design of steel plate shear walls*, Steel TIPS Report, Structural Steel Educational Council, July, Moraga, CA.

Berman, J. and Bruneau, M. (2003), "Plastic analysis and design of steel plate shear walls", *J. Struct. Eng.* ASCE, **129**, 1448-1456.

Budynas, R.G., (1977), *Advanced Strength and Applied Stress Analysis*, Mc Graw-Hill.

Caccese, V., Elgaaly, M. and Chen, R. (1993), "Experimental study of thin steel-plate shear walls under cyclic load", *J. Struct. Eng.*ASCE, **119**(2),573-587.

Canadian Standard Association, CAN/CSA S16-01, (2001), *Limit States Design of Steel Structures*, Toronto, Ontario.

Driver, R.G., Kulak, G.L., Kennedy, D.J.L. and Elwi, A.E. (1997), *Seismic behaviour of steel plate shear walls*, Structural Engineering Report No. 215, Department of Civil and Environmental Engineering, University of Alberta, Edmonton, Canada.

Driver, R.G., Kulak, G.L., Kennedy, D.J.L. and Elwi, A.E. (1998a), "Cyclic test of a four-storey steel plate shear wall", *J. Struct. Eng.* ASCE, **124**(2), 112-120.

Driver, R.G., Kulak, G.L., Elwi, A.E. and Kennedy, D.J.L. (1998b), "FE and simplified models of steel plate

shear wall", *J. Struct. Eng.* ASCE, **124**(2), 121-130.
Elgaaly, M., Caccese, V. and Du, C. (1993a), "Postbuckling behaviour of steel-plate shear walls under cyclic loads", *J. Struct. Eng*. ASCE, **119**(2), 588-605.
Elgaaly, M., Caccese, V. and Martin, D.K. (1993b), *Experimental investigation of the behaviour of bolted thin steel plate shear walls*, Civil Engineering Department, University of Main, Orono, Main.
Elgaaly, M., Caccese, V. and Du, C. (1994), "Closure to Postbuckling behaviour of steel-plate shear walls under cyclic loads", *J. Struct. Eng*. ASCE, **120**(7), 2251-2255.
Kennedy, D.J.L., Kulak, G.L. and Driver, R.G. (1994), "Discussion of Postbuckling behaviour of steel-plate shear wall under cyclic loads", *J. Struct. Eng.*ASCE, **120**(7), 2250-2251.
Kuhn, P., Peterson, J.P. and Levin, L.R. (1952), *A summary of diagonal tension, part I Methods of analysis*, Technical Note 2661, National Advisory Committee for Aeronautics, Washington, D.C.
Kulak, G.L., Kennedy, D.J.L. and Driver, R.G. (1994), "Discussion of Experimental study of thin steel-plate shear walls under cyclic load", *J. Struct. Eng.*ASCE, **120**(10), 3072-3073.
Lubell, A.S. (1997), *Performance of unstiffened steel plate shear walls under cyclic Quasi-static loading*, M.A.Sc. Thesis, Department of Civil Engineering, University of British Columbia, Vancouver, BC, Canada.
Lubel, A.S., Prion, H.G.L., Ventura, C.E. and Rezai, M. (2000), "Unstiffened steel plate shear wall performance under cyclic loading", *J. Struct. Eng*. ASCE, **126**(4), 453-460.
Reddy, J.N. (2002), *Energy Principles and Variational Methods in Applied Mechanics*, 2nd edition, Wiley.
Rezai, M. (1999), *Seismic behavior of steel plate shear walls by shake table testing*, PhD Dissertation, Department of Civil Engineering, University of British Columbia, Vancouver, BC, Canada.
Rezai, M., Ventura, C.E. and Prion, H.G.L. (2000), "Numerical investigation of thin unstiffened steel plate shear walls", *Proc., World Conf. of Earthquake Engineering*, pp. 0801-10801-8.
Shishkin, J.J., Driver, R.G. and Grondin, G.Y. (2005), *Analysis of steel plate shear walls using the modified strip model*, Structural Engineering Report No. 261, University of Alberta, Canada.
Smith, S.T., Bradford, M.A. and Oehlers, D.J. (1999), "Elastic buckling of unilaterally constrained rectangular plates in pure shear", *Eng. Struct.*, **21**, 443-453.
Thorburn, L.J., Kulak, G.L. and Montgomery, C.J. (1983), *Analyses of steel plate shear walls*, Structural Engineering Report No. 107, University of Alberta, Canada 1983.
Timler, P.A. and Kulak, G.L. (1983), *Experimental study of steel plate shear walls*, Structural Engineering Report No. 114, Department of Civil Engineering, University of Alberta, Edmonton, Canada.
Timoshenko, S. and Gere, J.M. (1963), *Theory of Elastic Stability*, Mc Graw-Hill, New York, USA.
Tromposch, E.W. and Kulak, G.L. (1987), *Cyclic and static behaviour of thin steel shear walls*, Structural Engineering Report No. 145, Department of Civil Engineering, University of Alberta, Edmonton, Canada.
Varadan, T.K. and Bhaskar, K. (1999), *Analysis of Plates*, Narosa Publishing House, New Delhi, India.
Wagner, H. (1931), *Flat sheet metal girders with very thin webs, Part I-General theories and assumptions*, Technical Memo No. 604, National Advisory Committee for Aeronautics, Washington, D.C.

BU

Appendix

$\mathbf{K}_0$ is the linear stiffness matrix whose argument of The i-th row and j-th column ($K_0(i,j)$) given by:

$$K_0(i,j) = K_0^P(i,j) + K_0^{st}(i,j) + K_0^{sf}(i,j)$$

where $K_0^P(i,j)$ is the plate stiffness matrix and $K_0^{st}(i,j), K_0^{sf}(i,j)$ are the torsional and out-of-plane flexural stiffness matrices related to the springs, respectively as below:

$$K_0^P(i,j) = \iint \{D[\phi_{,xx}(i)\phi_{,xx}(j) + \phi_{,yy}(i)\phi_{,yy}(j)] \\ + D\nu[\phi_{,xx}(i)\phi_{,yy}(j) + \phi_{,yy}(i)\phi_{,xx}(j)] + 2D(1-\nu)(\phi_{,xy}(i)\phi_{,xy}(j))\}\,dxdy$$

$$K_0^{st} = K_{tor}\left(\begin{array}{l} \int\left([\phi_{,x}(i)\phi_{,y}(j)]\big|_{x=-\frac{a}{2}} + [\phi_{,x}(i)\phi_{,y}(j)]\big|_{x=\frac{a}{2}}\right)dy \\ + \int\left([\phi_{,y}(i)\phi_{,y}(j)]\big|_{y=-\frac{b}{2}} + [\phi_{,y}(i)\phi_{,y}(j)]\big|_{y=\frac{b}{2}}\right)dx \end{array}\right)$$

$$K_0^{sf} = K_{flx}\left(\begin{array}{l} \int\left([\phi_{,y}(i)\phi_{,y}(j)]\big|_{x=-\frac{a}{2}} + [\phi_{,y}(i)\phi_{,y}(j)]\big|_{x=\frac{a}{2}}\right)dy \\ + \int\left([\phi_{,x}(i)\phi_{,x}(j)]\big|_{y=-\frac{b}{2}} + [\phi_{,x}(i)\phi_{,x}(j)]\big|_{y=\frac{b}{2}}\right)dx \end{array}\right)$$

in which $\phi(i)$ is the i-th argument of Φ. Also $\mathbf{K_G}$ is the geometric stiffness matrix whose argument of the i-th row and j-th column ($\mathbf{K_G}(i,j)$) is expressed by:

$$K_G(i,j) = \iint [\phi_{,x}(i)\phi_{,y}(j) + \phi_{,y}(i)\phi_{,x}(j)]\,dxdy$$

Notations

A	: area of plate
$\mathbf{a}$	: eigenvector whose arrays are Ritz coefficients
a	: width of plate
a_{1m}, a_{2n}, a_{3l}	: arbitrary Ritz coefficients
b	: height of plate
D	: flexural rigidity of isotropic plate
E	: Young's modulus
f_1	: number of degrees of freedom for two-dimensional polynomial
f_2, f_3	: numbers of degrees of freedom for one-dimensional polynomials

G	: shear modulus of elasticity
$\mathbf{K}_0$	: linear stiffness matrix
$\mathbf{K_G}$	: geometric stiffness matrix
K_{flx}	: unit length out-of-plane flexural rigidity of surrounding members
K_{tor}	: unit length torsional rigidity of surrounding members
k_s	: shear buckling coefficient
N_{xy}	: elastic shear buckling load
p	: degree of a two-dimensional polynomial
U	: elastic strain energy of system
U_p	: elastic strain energy of plate
U_s	: elastic strain energy of springs
V_p	: geometric strain energy of system
w	: lateral buckling displacement of plate
α	: relative torsional stiffness of surrounding members
β	: relative out-of-plane flexural stiffness of surrounding member
$\mathbf{\Phi}$	: square matrix whose arrays are polynomials
ϕ_{1m}	: two-dimensional polynomial
ϕ_{2n}, ϕ_{3l}	: one-dimensional polynomials
ϕ_{b1}, ϕ_{b2}, ϕ_{b3}	: boundary polynomials
ν	: Poisson's ratio
Π	: total potential energy of system
θ	: angle of inclination of strips related to columns
σ_x, σ_y	: normal stresses due to out-of-plane displacements of plate
τ_{xy}	: shear stress due to out-of-plane displacements of plate